Local atomic and electronic arrangements in $W_xV_{1-x}O_2$

C. Tang, P. Georgopoulos, M. E. Fine, and J. B. Cohen
Department of Materials Science and Engineering, The Technological Institute, Northwestern University, Evanston, Illinois 60201

M. Nygren
Department of Inorganic Chemistry, Arrhenius Laboratory, University of Sweden, 10691 Stockholm, Sweden

G. S. Knapp and A. Aldred
Materials Science and Technology Division, Argonne National Laboratory, Argonne, Illinois 60439
(Received 27 August 1984)

Low-temperature magnetic susceptibilities yield an effective magnetic moment per W atom of $(3.24\pm0.10)\mu_B$ for both $W_{0.05}V_{0.95}O_2$ and $W_{0.08}V_{0.92}O_2$. This value suggests a transfer of two d-shell electrons from the W to neighboring V ions to form V^{3+}-W^{6+} and V^{3+}-V^{4+} pairs along the a axis of the monoclinic low-temperature phase. Studies of the extended x-ray-absorption fine-structure pattern for various compositions of different W-cation fraction x, and of the area of the W L_{III}-edge resonance as well, confirm that the valence of W is 6+. Also, examination of the position of the V K edge versus composition for these alloys and other compounds indicates that the concentration of V^{3+} ions increases with W-cation fraction x. Thus, upon alloying VO_2 with W, the reduction in the temperature of the metal-semiconductor transition by W appears to be due to charge transfer. From x-ray small-angle scattering it was found that there are no W-atom clusters present. The high-field magnetization at low temperature suggests that alloying causes this oxide to become a spin glass.

INTRODUCTION

The compound VO_2 is one of several oxides that undergoes a metal-semiconductor transition. At $T_c=341$ K, its conductivity increases by 5 orders of magnitude.[1-3] Above T_c, the metallic phase has the rutile structure. In the low-temperature semiconductor phase, pairs of V ions form; within a pair, the spacing is 2.65 Å, while the ions in the next pair are at a distance of 3.12 Å.[4] The pairs are not collinear with the c axis of the rutile phase, but form a zigzag array in this (monoclinic) structure. Goodenough[5] has suggested that the single $3d$ electron on each V ion is involved in a homopolar bond to form these V "molecules" below T_c. However, this would lead to residual diamagnetism, whereas VO_2 exhibits a weak (temperature-independent) paramagnetism.[6,7] Accordingly, various band models have been proposed.[8,9-12] The importance of electron-electron interaction has also been stressed.[13]

The magnetic susceptibility in the metallic phase is nearly an order of magnitude greater than that for the low-temperature phase. Various proposals for the band structure of this high-temperature structure have been made, including a two-band scheme,[14] and one based on overlapping Mott-Hubbard bands.[15]

While the band point of view is clearly the most appropriate for VO_2, it is not so clear what the most useful model to describe the changes in the system due to alloying is. Rather dramatic changes occur in alloying with $_{74}W$, $_{41}Nb$, $_{42}Mo$, etc. In this paper we investigate the substitution of W for V in VO_2. We measure magnetization, small-angle x-ray scattering (SAXS), extended x-ray-absorption fine structure (EXAFS), and x-ray-absorption near-edge structure (XANES) in order to understand the local electronic and atomic structures of these alloys. We find that it is possible to describe the magnetic results in terms of a local model in which coupled pairs of atoms form "local moments." In addition, we find it useful to think of V and W as having definite valences. Because of electron correlations, the effective charges and moments may be reasonably localized. Indeed, this seems to be the case when Nb is the alloying element, for which a charge-hopping model and a spin cloud have been suggested.[16] Local moment and the valence concepts are useful to discuss our results for W, and for that reason we will use them.

Doping is one method for probing the exact nature of the interactions in such a system. Indeed, the effects of such dopants can be quite large. The transition temperature decreases at a rate of 26 K/at.% W, but only 11 K/at.% Nb or Mo.[7,17-24]. Substitution of solute markedly decreases the jump in resistivity as well, and alters the magnetic susceptibility.[7,17-20] When either W or Nb is added to VO_2, the paramagnetic susceptibility of the low-temperature phase increases, and this phase exhibits Curie-Weiss behavior. There is some indirect evidence for clustering of the solute from the curvature of magnetization versus applied field for the case of W.[25] In the latter investigation, this curvature was analyzed in terms of superparamagnetic clusters, but data are required over a much larger range of applied field in order to confirm the superparamagnetism. While doping clearly alters the

properties of this oxide, the reasons for the changes are not as yet clear, nor is it apparent why the behavior is so different for different solute species.

In the present investigation, small-angle x-ray scattering, near-edge spectroscopy, and magnetization were employed to elucidate the role of tungsten on the transition in VO_2.

EXPERIMENTAL PROCEDURES

Sample preparation

W-doped VO_2 with W-cation fractions x of 0.05, 0.08, 0.11, 0.25, and 0.33 were prepared by thoroughly mixing appropriate portions of high-purity powders of V_2O_5, V_2O_3, and WO_2, sealing in evacuated silica capsules, and firing at 1273 K for 11—12 d. Compositions were obtained by comparing the lattice parameters with published values.[18,21,26]

Magnetic measurements

Magnetization curves were obtained with two Faraday balances[27] at Argonne National Laboratory. With one balance, fields up to 1.4 kG could be obtained from 3.5 to 300 K. The data were obtained automatically at a given temperature at a series of seven increasing and seven decreasing fields. The second balance employed superconducting coils, and fields up to 90 kG could be obtained from 2 to 90 K. Both balances were calibrated with single-crystal nickel, the magnetization of which is well established.

Small-angle x-ray scattering

The x-ray source was a 12-kW Rigaku rotating-anode generator with a molybdenum target. Point collimation was employed, and the outer edge of the parasitic scattering was at an angle of $0.25°=2\theta$. The detector was a Tennelec position-sensitive proportional counter with flowing P-10 gas at 6 atm pressure. To examine the effects of using the powdered specimens employed in this study, Al powders of various sizes were also measured. Foils and powders of quenched and aged Al—5.2 at. % Zn were examined as well because the coherent miscibility gap is well established.[28] Therefore, the compositions of the phases present and their amounts are known for any temperature, and the scattering can be employed to obtain the intensity of the incident beam. With this value, the scattered intensities for various models of the oxide can be calculated to compare to data on an absolute scale.

By using filtered Mo $K\alpha$ radiation, it was possible to use samples of significant thickness (generally one or two absorption thicknesses, that is between 0.4 and 0.8 mm), whereas Cu $K\alpha$ radiation would have required one-sixth of this thickness; this is difficult to achieve with powders. For each sample, four SAXS patterns were measured, namely (1) SAXS from the sample in the sample holder (which had thin polyethylene windows), (2) the pattern from the empty sample holder, (3) SAXS from the sample in the holder plus a polyethylene plate, and (4) the pattern from the empty holder plus the plate. By comparing the integrated intensity of the polyethylene peak at $\sim 3°=2\theta$ for runs 3 and 4, the absorption coefficient of the sample, μ, was obtained:

$$\exp(-\mu t)=I_3/I_4 \ . \tag{1}$$

The net intensity scattered by the sample is then equal to

$$I_{\text{net}}=I_1-[I_2\exp(-\mu t)] \ . \tag{2}$$

EXAFS and XANES

Both extended x-ray-absorption fine structure and x-ray-absorption near-edge structure were examined at CHESS (the Cornell University High Energy Storage Ring Source), and on an in-house facility. At CHESS, the energy of the incident energy was varied with a channel-cut Si crystal [(220) reflection] with a "weak" link, so that, by detuning, harmonics can be reduced to 1% or less of the desired energy. To calibrate the energy, the values of the K absorption edge of Fe was employed for the range between 6 and 10 keV, and the L_{III} edge of Pt for the range 10—15 keV. For XANES (at the W L_{III} edge), the energy range from -50 eV $+E_0$ to 150 eV $+E_0$ was sampled at 0.5-eV intervals. For EXAFS (also at the W L_{III} edge) the range was -100 eV $+E_0$ to 800 eV $+E_0$. The energy resolution was 2 eV.

The in-house source, employed for XANES near the V K edge, was a Rigaku 12-kW rotating-anode generator with a Mo target. Elastically bent Si crystals mounted on a standard diffractometer were employed to select the incident energy, and this was varied by changing the scattering angles. Two gas-flow proportional counters, one with a 12-mm active length located before the sample and one 51 mm long located after the sample, were used to measure the absorption coefficient, by taking the logarithmic ratio of the two readings normalized by the respective detector efficiencies. By varying the fill gas (P-10) pressure, the first detector was made to absorb about 10% of the beam, whereas the second detector was about 35% efficient. With this scheme, saturation of the second detector was avoided, and absorption by this detector of the half-wavelength component was greatly reduced. (A pulse-height analyzer was also employed to further reduce harmonics.) Fast-pulse-counting electronics were employed; the slowest elements were the single-channel analyzers, which had a pulse-pair resolution of 100 ns. A current-feedback controller was installed on the x-ray generator to keep the incident intensity constant regardless of energy.[29] An energy resolution of ~ 2 eV at the V K edge was obtained with a Si (220) reflection and a receiving slit of 0.025 mm. Data were taken at intervals at 0.5 eV.

While it took only 15—20 min to obtain good spectra at CHESS, it took 2—3 h on the in-house facility. The results on the two devices were quite comparable.[30,31]

Analyses of EXAFS data proceeded as follows. Data above the absorption edge $\mu(k)$ were smoothed iteratively (50 times), and the smoothed value, $\mu_0(k)$, was subtracted from the actual absorption (which contained the EXAFS oscillations). The data below the edge were fitted to a Victoreen formula, extrapolated above the edge [$\mu_0^1(k)$], and subtracted from the smooth values there. This differ-

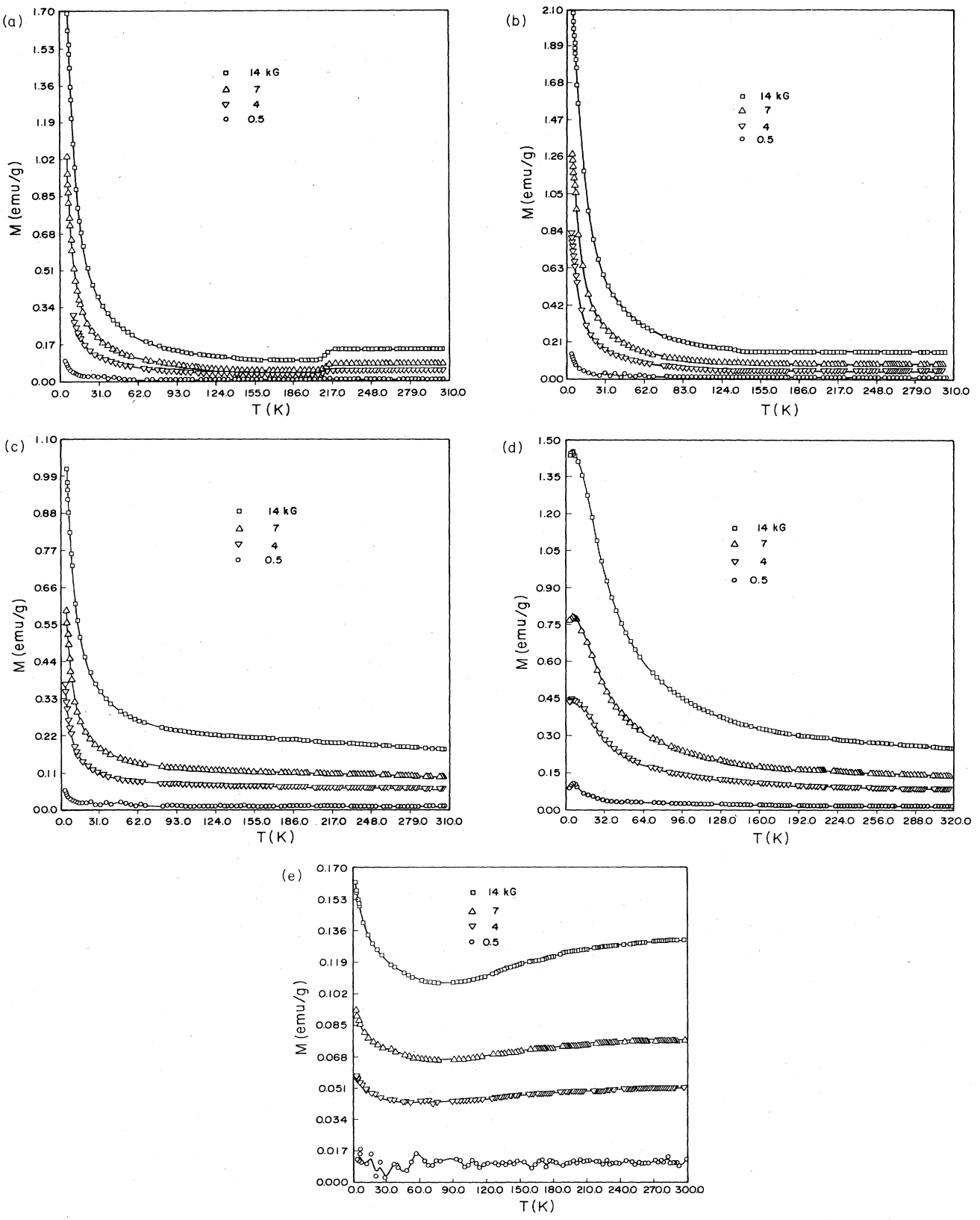

FIG. 1. M vs T. Each line represents one field. (The corresponding field is indicated.) (a) $W_{0.05}V_{0.95}O_2$. (b) $W_{0.08}V_{0.92}O_2$. The transition temperature is near 135 K. (c) $W_{0.11}V_{0.89}O_2$. (d) $W_{0.25}V_{0.75}O_2$. (e) $W_{0.33}V_{0.67}O_2$. This material has a tri-rutile structure and has been reported to have a Néel temperature (T_N) of 370±30 K. (The increase of M at low temperature might be due to impurities.)

ence was used to normalize the first difference. After multiplying by a power of the ejected electron's wave vector, k^n, and multiplying by a Gaussian-broadened square window function[32] to minimize the effects of the limited k range of EXAFS data, the data were Fourier-transformed. Peaks in the resulting radial distribution function (RDF) were isolated with a similar window and back-transformed. The resulting single-shell EXAFS spectra were analyzed (for each shell around the absorbing species) with the following equation for the EXAFS oscillations $\chi(k)$:

$$\chi(k)=[\mu(k)-\mu_0(k)]/[\mu_0(k)-\mu_0^1(k)] = \sum_j [N_jF_j(k)/kR_j^2]\sin[2kR_j+\phi_j(k)] \times\exp(-2k^2\sigma_j^2)\exp(-2R_j/\lambda) . \quad (3)$$

A nonlinear least-squares-fitting procedure was employed for the terms R_j, the neighbor distance, the Debye-Waller factor σ_j, the shift of the edge E_0 (since $k=[2m(E-E_0)/\hbar^2]^{1/2}$), and the term

$$A_j=N_j\exp(-2R_j/\lambda_j) ,$$

where N_j is the number of neighbors of type j at R_j, and λ_j is the mean free path of the backscattered electrons. The calculated values of Teo and Lee[33] were employed for the scattering amplitudes $F_j(k)$ and the phase shifts $\phi_j(k)$. The fit was accomplished by Gauss-Jordan reduction, employing a Householder transformation with optimization.[34]

For XANES at a K edge, the energy of the edge (E_0) was established as the first inflection point on the main jump in absorption. The data were normalized by the jump at the edge, which was determined by extrapolating the data above and below the edge to E_0. An L edge exhibits a large resonance peak due to transition from a core level to vacant d states.[35] Lytle *et al.*[36] have related the difference in area of this peak, in the pure metallic state and that for the same element in a compound, to differences in the number of d vacancies in these two states. To obtain this area the data were first normalized as described above, and then the energy of the edge for a compound was shifted so that the spectra of the compound and metal were matched just below the edge. Then the area of the peak in the difference spectra was evaluated.

RESULTS AND DISCUSSION

Magnetic studies

Portions of the curves of M vs T for various fields are shown in Fig. 1. For the 5% W-cation case, there is an increase in M upon heating at 205 K associated with the transition from the low-temperature semiconductor phase to the metallic state, whereas for the 8% W-cation case there is a decrease at 135 K, and the transition occurs over a broader range of temperatures than for the 5% W-cation case. (This difference has not been reported before.) There is no sign of the transition, at least above 3.5 K, for the 11% W-cation alloy, in agreement with extrapolations of published data.[25]

TABLE I. Curie-Weiss constants, $10\text{ K} < T < T_c$.

5% W cation		8% W cation	
C (emu K/mole)	Θ (K)	C (emu K/mole)	Θ (K)
6.7×10^{-2}	−0.7	1.1×10^{-1}	−1.1

The compound WV_2O_6 (33% W cation) has an antiferromagnetic interaction at 370 K,[37] and therefore our data for this material show a gradual decrease in M with decrease in temperature. This was also evident for the 25% W-cation alloy below about 7 K, so that this composition probably has a structure similar to WV_2O_6, at least locally.

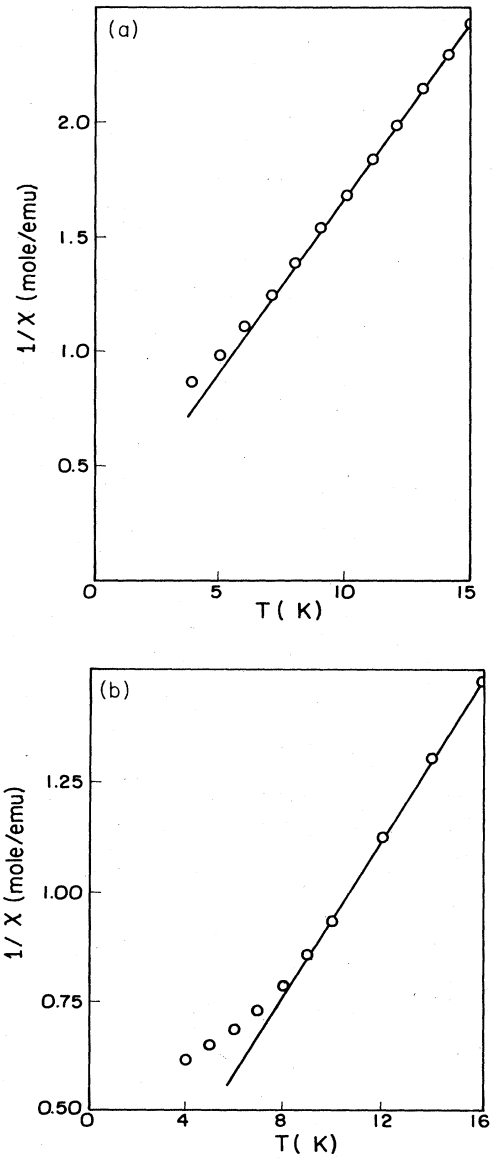

FIG. 2. $1/\chi$ vs T. (a) $W_{0.05}V_{0.95}O_2$. (b) $W_{0.08}V_{0.92}O_2$.

The initial susceptibility χ for the 5% W-cation alloy agrees with Ref. 18 to within 1% at both 77 and 300 K. The solute susceptibility χ_m fits a Curie-Weiss law in the region of 10 K $< T < T_c$:

$$\chi_m = \chi - \chi_0 = C/(T-\Theta)\ , \tag{4a}$$

where χ_0 is the susceptibility of pure VO_2, C is the Curie constant, and Θ is the Curie-Weiss temperature. The terms for such a fit to the data are given in Table I. At very low temperatures, the data deviate from this behavior (Fig. 2), which suggests that there may be a spin-glass transition below 1 K. We will return to this point below. From Table I the effective magnetic moment per W atom, $\mu_{\rm eff}$, can be calculated for 10 K $< T < T_c$:

$$\mu_{\rm eff} = g\mu_B[S(S+1)]^{1/2} = (3k_BC/N)^{1/2}\ . \tag{4b}$$

Here, N is the number of W ions per mole, k_B is

TABLE II. Magnetic susceptibilities near T_c.

$[\chi(<210\ \text{K})]_{5\%\ \text{W cation}} = 500\times10^{-6}$ emu/mole
$[\chi(<125\ \text{K})]_{8\%\ \text{W cation}} = 980\times10^{-8}$ emu/mole
$[\chi(>210\ \text{K})]_{5\%\ \text{W cation}} = 800\times10^{-6}$ emu/mole
$[\chi(>125\ \text{K})]_{8\%\ \text{W cation}} = 900\times10^{-6}$ emu/mole

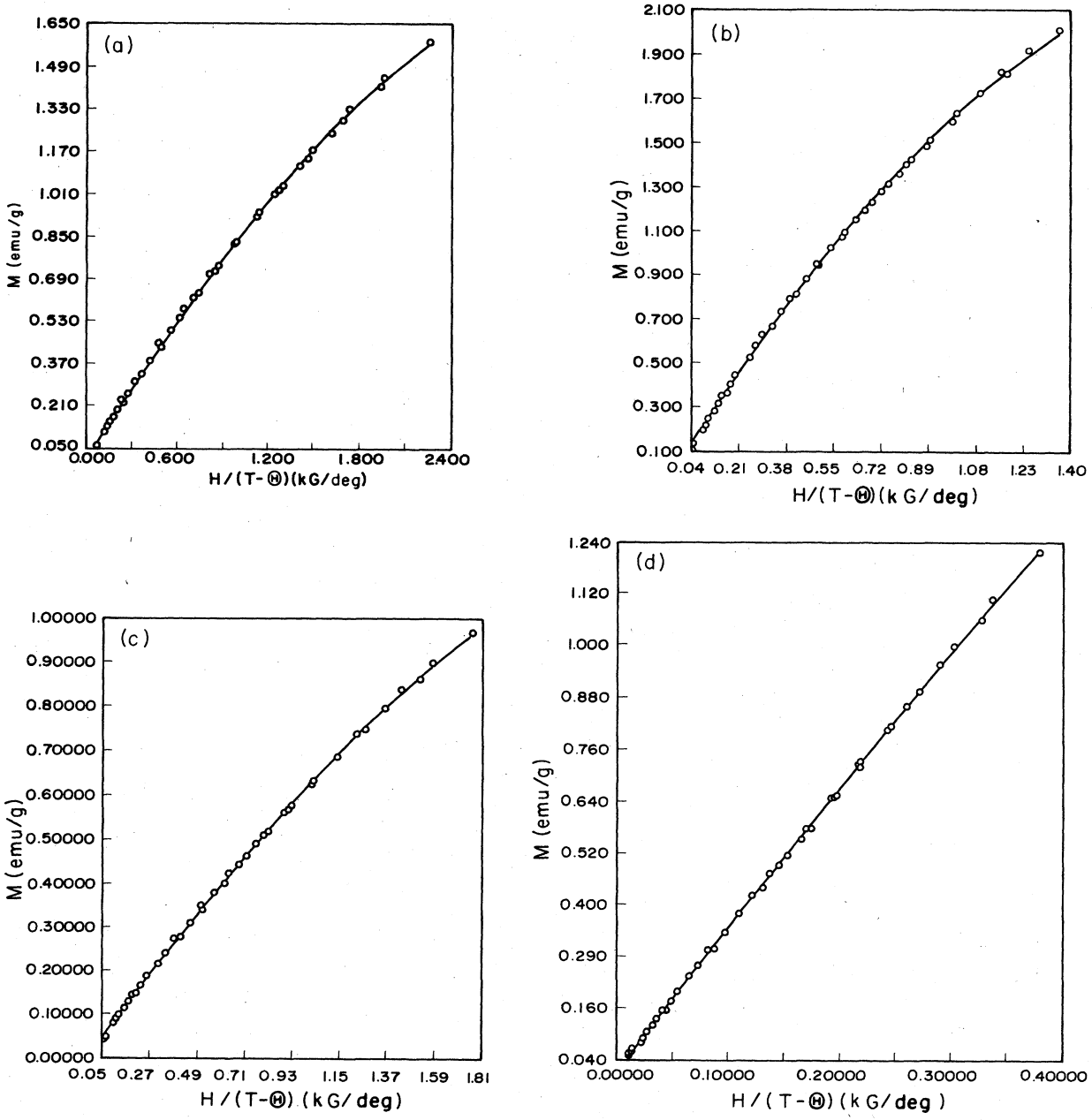

FIG. 3. M vs H at 4–6 K. (a) 5% W cation. (b) 8% W cation. (c) 11% W cation. (d) 25% W cation.

TABLE III. Weiss temperature Θ, average spin J, and average particle number N, from the fit to low-field data on $W_xV_{1-x}O_2$.

Sample	Weiss temperature Θ	Spin number J	Number of particles (10^{21}/mole of sample)
$W_{0.05}V_{0.95}O_2$ (4–6 K)[a]	−1.94	6.38	2.00
$W_{0.08}V_{0.92}O_2$ (4–6 K)[a]	−6.47	12.31	1.29
$W_{0.11}V_{0.89}O_2$ (4–6 K)[a]	−5.62	7.10	1.32
$W_{0.25}V_{0.76}O_2$ (25–35 K)[a]	−20.6	16.54	1.61
$W_{0.05}V_{0.95}O_2$ (4–6 K and 0–76 kG)[a]	−1.89	7.21	1.50
$W_{0.05}V_{0.95}O_2$ (4–45 K and 10 kG)[a]	−1.78	6.15	2.12

[a]These values indicate the temperature and field range of the data being fitted.

Boltzmann's constant, and S is the spin per atom. The spectroscopic splitting factor $g=2$,[25] and the value of μ_{eff} is $(3.24\pm10)\mu_B$ for both the 5% and 8% W-cation alloys. This value is nearly equal to that for a combination of two spins, $S_1=1$ and $S_2=\frac{1}{2}$:

$$\mu_{\text{eff}}=g\mu_B[S_1(S_1+1)+S_2(S_2+1)]^{1/2}=3.32\mu_B\ . \tag{4c}$$

This result suggests that each added W ion breaks up a V^{4+}–V^{4+} homopolar bond and causes the transfer of two $3d$ electrons to the nearest V ions for charge compensation, forming two new bonds, namely V^{3+}–W^{6+} and V^{3+}–V^{4+}. The V^{3+}-W^{6+} pair has two electrons with parallel spin in triplet-spin states, so that $S=1$, while there is only one $3d$ electron in the V^{3+}-V^{4+} pair, the other two forming the bond. On this basis, the changes in the magnetization at T_c can be explained. The magnetic susceptibility below T_c can be calculated:

$$\chi(T<T_c)=\{Ng^2\mu_B^2[S_1(S_1+1)+S_2(S_2+1)]\}/3k_B(T-\Theta)\ . \tag{5}$$

The calculated values just below the transition are given in Table II. For the high-temperature phase, each percent of W adds $\sim30\times10^{-6}$ emu/mole to the value for pure VO_2,[18] so that the values just above T_c are those also reported in Table II. Since χ for the 8% W-cation sample at $T<T_c$ is larger than the value above T_c, an increase in the magnetic susceptibility occurs upon dropping below the transition; the reverse occurs for the 5% W-cation alloy.

The M-vs-H data are shown in Fig. 3 for some of the temperatures examined. A slight curvature is evident, and following Langill[25] we attempted to analyze this data using superparamagnetic theory.[38–41] The material was assumed to contain small weakly interacting magnetic regions. With N, the number of such regions per gram, J their spin, and B the Brillouin function,

$$M=Ng\mu_B B(x'')\ , \tag{6a}$$

$$x''=gJ\mu_B H/[k_B(T-\Theta)]\ . \tag{6b}$$

These equations were employed to fit the data over the range 0–14 kG, 4–6 K for the 5%, 8%, and 11% W-cation alloys, and 20, 25, and 35 K for the 25% W-cation alloy (to avoid the antiferromagnetic transformation). Least-squares results for N, J, and the Curie-Weiss temperature Θ are given in Table III. The fit to the data over these fields is shown in Fig. 3. The cluster size (indicated by J in Table III) is smaller than that in Ref. 25, but similar in magnitude. Attempts at similar fits to the high-field data were unsuccessful,[30] and the parameters determined from the low-field data do not fit the high-field results, Fig. 4. Several other procedures were tried:[30] (1) a

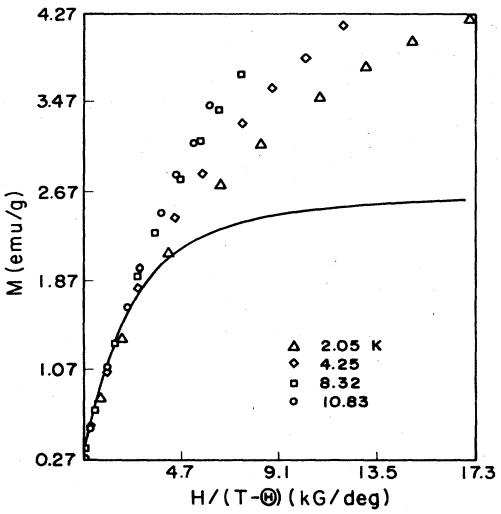

FIG. 4. 5% W-cation sample, M vs H. Symbols, high-field data; solid line, prediction from the low-field fitting parameters.

TABLE IV. Fitting parameters $\chi_0(T)$ and $b(T)$, as well as root-mean-square residual and T_c [calculated from $b(T)$, Eq. (7)].

T (K)	$\chi_0(T)$ (10^{-5} emu/g)	$b(T)$ (10^{-11}g/G)	rms residual (10^{-1})	$1/\chi_0(T)$ (10^4)	T_c (K)
2.05	9.62 (±18%)	7.75 (±30%)	2.60	1.04	1.04
4.25	8.53 (±10%)	6.71 (±30%)	1.81	1.17	3.04
8.32	6.62 (±5%)	5.08 (±20%)	7.05	1.51	6.94
0.83	5.41 (±2%)	3.22 (±20%)	3.96	1.85	8.83

mean internal field was included in the argument of the Brillouin function; (2) following Beck,[42] three cluster sizes were assumed to be present and the data were fitted to N_i, J_i, and Θ_i for all three sizes; and, finally, (3) the particles were assumed to be uniaxially anisotropic,[43,44] and the data were fitted to the magnetic moment per particle, the number of particles, the anisotropic energy, and an internal field. These various approaches failed to improve the fit to the data when the adjustable parameters were determined from one field range and applied to the other, or the parameters were so highly correlated that results were meaningless. The data on the low-temperature susceptibility presented above suggested that these ceramic alloys are spin glasses, with a transition temperature T_g below our measurement range. Sherrington and Kirkpatrick[45] have derived an equation for the magnetization for a spin glass based on an Ising model in which spins are coupled by infinite-range random interactions, distributed with a Gaussian probability. Monud and Bouchiat[46] expanded the resultant equations for use above T_g, and we have employed these expansions, with M the saturation magnetization:

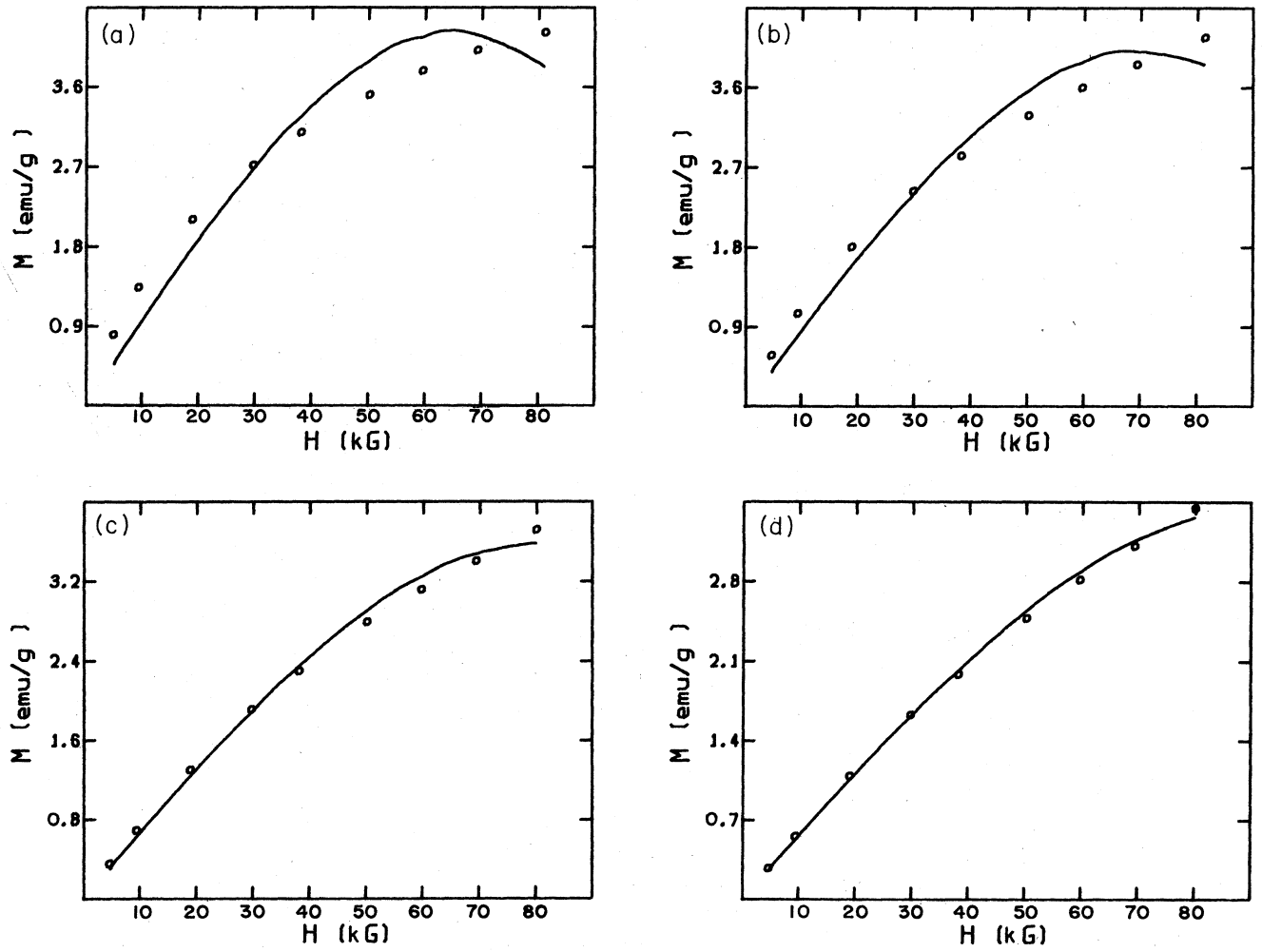

FIG. 5. (a) Fit of Eq. (7) to $M(H,T)$, 5% W-cation sample. (a) $T=2.05$ K, (b) 4.25 K, (c) 8.32 K, and (d) 10.83 K. Circles, data; line, Eq. (7).

$$M(T)=\chi_0(T)[1-b(T)H^2]H\ , \tag{7a}$$

$$\chi_0=M_0/k_BT\ , \tag{7b}$$

$$b(T)=(T^2+2T_g^2)/[3k_B^2T^2(T^2-T_g^2)]\ . \tag{7c}$$

The fit to the data is given in Table IV and Fig. 5. This fit is the best of all the models attempted over the entire range of H. Thus, it indeed appears that there is a spin-glass transition at ~ 1 K. (The variation in T_g in the table is probably a result of the fact that higher-order terms were neglected in the equations employed.)

In summary, the magnetic data suggest that there is an electron transfer for charge compensation between W and V ions, and that leads, at low temperature, to spin-glass behavior. In order to confirm whether or not this transfer actually occurs, near-edge spectroscopy was employed, and to examine whether or not (W-rich) magnetic clusters are present, small-angle x-ray patterns were obtained.

Small-angle x-ray scattering

To place these measurements on an absolute scale, the scattering from a foil of Al—5.2 at. % Zn was measured, after a solution treatment at 698 K, a water quench, and a long aging at room temperature to produce the equilibrium volume fraction of Guinier-Preston zones whose composition is known.[28] The power in the direct beam, P_0, was obtained from the intensity of this specimen, $I(h)$, where $h=4\pi(\sin\theta)/\lambda$:

$$P_0=[Q/(2\pi)^2]I_e\exp(-\mu t)p^{-2}(\Delta P)^2V_{\rm irr}c(1-c)\ , \tag{8a}$$

where

$$Q=4\pi\int_{-\infty}^{+\infty}h^2I(h)dh\ , \tag{8b}$$

and c is the volume fraction of zones, I_e is the scattering cross section of one electron, $V_{\rm irr}$ is the irradiated volume, p is the distance from the sample to the detector, and ΔP is the difference in electron density between zones and matrix. With the result $P_0=1.05\times10^6$ Hz, the pattern from the foil was calculated with the well-known Guinier formula:

$$I(h)=P_0I_ep^{-2}\exp(-\mu t)(V_p\,\Delta P)^2Ni(h)\ . \tag{9}$$

Here, V_p is the zone volume, $(4/3)\pi R^3$, where R was obtained from the radius of gyration, N is the number of particles irradiated, and $i(h)$ is the scattering by one

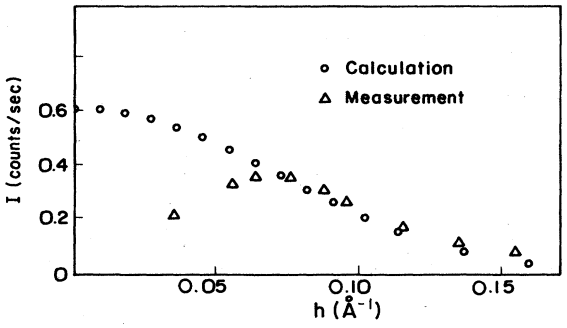

FIG. 6. Comparison between theoretical calculation and measurement of the SAXS of Al—8 wt. % Zn.

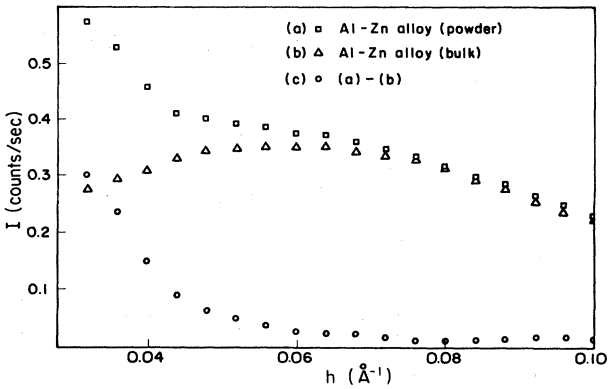

FIG. 7. Comparison of SAXS pattern of Al—8 wt. % Zn powder and Al—8 wt. % Zn bulk sample.

spherical zone, $\frac{9}{2}J_{3/2}(hR)/(hR)^{3/2}$. The radius of gyration was obtained from the initial slope of $\ln I$ vs h^2. The agreement with the measurements was excellent beyond the interference maximum, as shown in Fig. 6. When these measurements were repeated with a powder of the alloy, Fig. 7, there was a large rise in the scattering for $h<\sim0.06$. This was also detected (with the same magnitude) with pure Al powders sieved to the same size (<19 μm), and thus this phenomenon is due to refraction.[47,48] In what follows we will ignore this region. Three W-doped samples were examined, namely the 5%, 8%, and 25% W-cation oxides. The data for the first alloy are shown in Fig. 8. Also shown are the calculated intensities for a random solid solution with solute concentrations x:

$$i(h)=x(1-x)(\Delta f)^2 \tag{10}$$

(where Δf is the difference between atomic-scattering am-

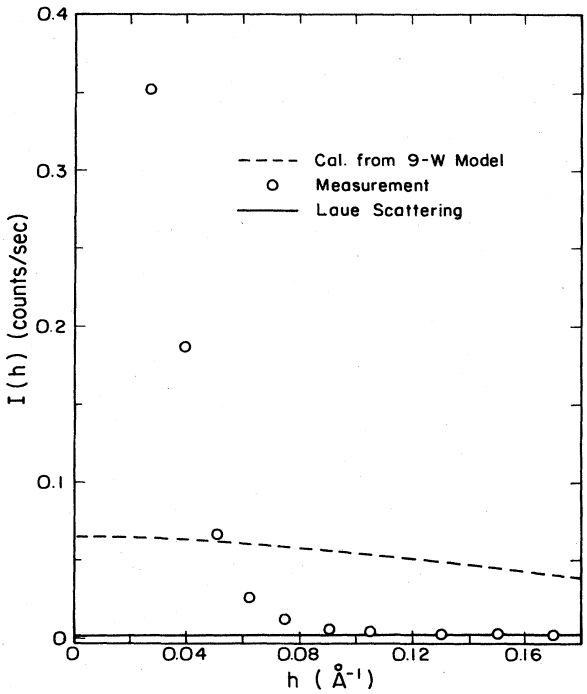

FIG. 8. Small-angle scattering, $W_{0.05}V_{0.95}O_2$.

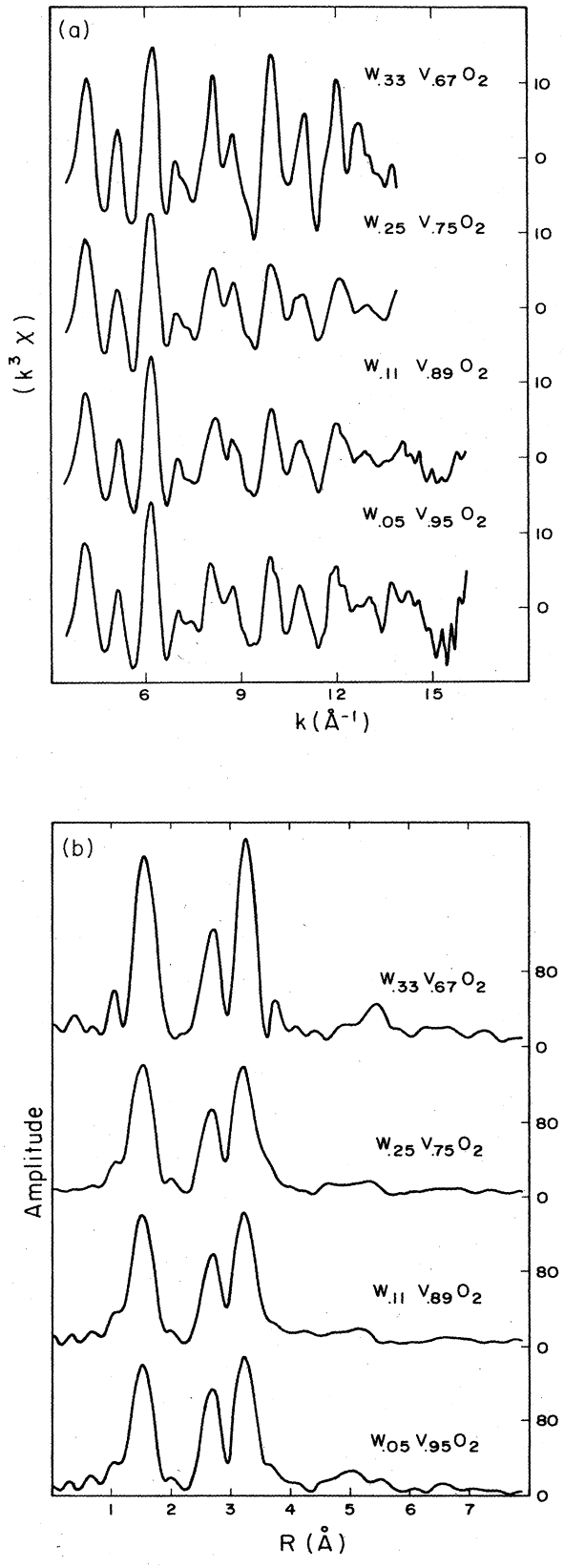

FIG. 9. (a) $k^3\chi(k)$ vs k, W-doped VO_2, near W L_{III} edge. (b) RDF, W-doped VO_2.

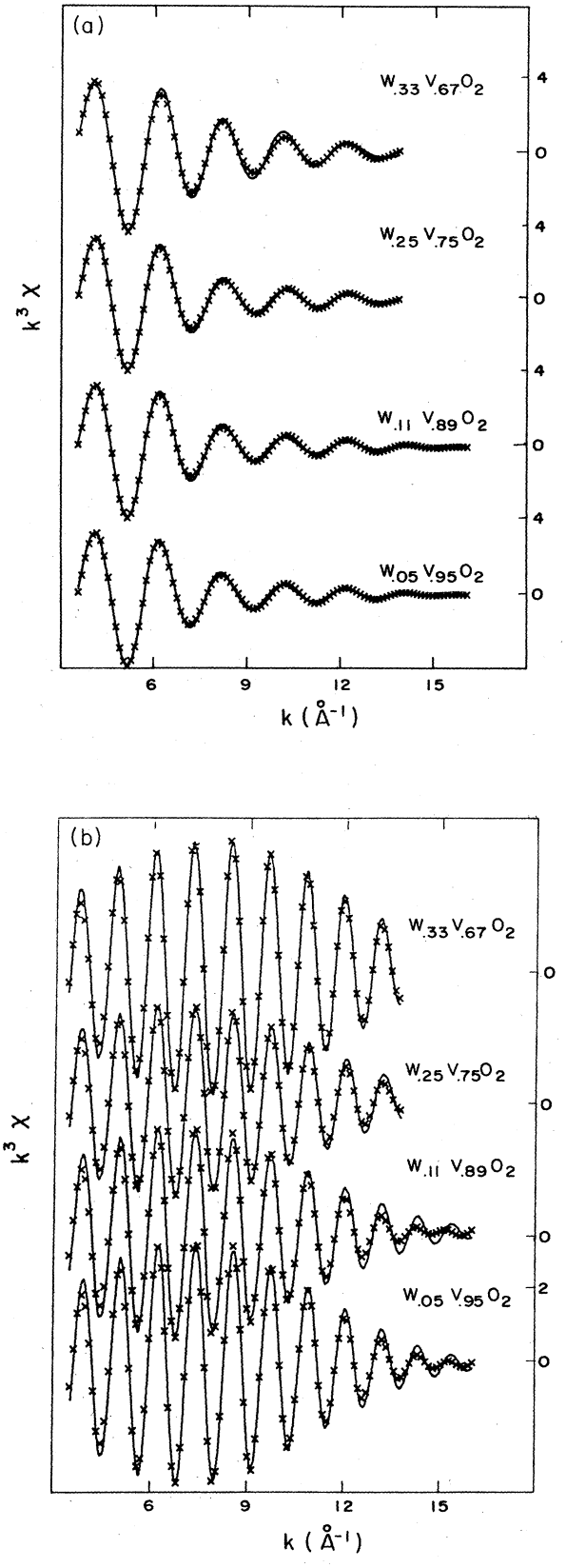

FIG. 10. (a) Fit of $k^3\chi(k)$ to the first shell (W-O): Experiment, solid line; fit, crosses. (b) Fit of $k^3\chi(k)$ to the second shell (W-V): Experiment, solid line; fit, crosses.

TABLE V. Fitting parameters and EXAFS spectra near W L_{III} edge.

Sample	Atom pair	Amplitude[a]	Distance, R (Å)	Distance from lattice parameters (Å) (Ref. 5)	σ^2	E_0 shift	R factor[b]
			First shell				
$W_{0.33}V_{0.67}O_2$	W-O	2.20 (±0.07)	1.92 (±0.01)	1.971	0.032 (±0.001)	19.6 (±0.3)	0.110
$W_{0.25}V_{0.75}O_2$	W-O	2.09 (±0.02)	1.91 (±0.01)	1.961	0.055 (±0.001)	18.0 (±0.1)	0.046
$W_{0.11}V_{0.89}O_2$	W-O	2.16 (±0.02)	1.91 (±0.01)	1.940	0.058 (±0.001)	19.1 (±0.1)	0.063
$W_{0.05}V_{0.95}O_2$	W-O	2.13 (±0.02)	1.92 (±0.01)	1.930	0.056 (±0.001)	19.6 (±0.1)	0.054
			Second shell				
$W_{0.33}V_{0.67}O_2$	W-V	2.06 (±0.02)	3.00 (±0.01)		0.075 (±0.001)	11.3 (±0.1)	0.040
$W_{0.25}V_{0.67}O_2$	W-V	2.54 (±0.04)	3.00 (±0.01)		0.101 (±0.001)	10.8 (±0.1)	0.095
$W_{0.11}V_{0.89}O_2$	W-V	2.56 (±0.05)	3.01 (±0.01)		0.099 (±0.001)	12.2 (±0.2)	0.113
$W_{0.05}V_{0.95}O_2$	W-V	2.59 (±0.04)	3.01 (±0.01)		0.092 (±0.001)	12.2 (±0.1)	0.078

[a]The amplitude is $N\exp(-2R/\lambda)$, where N is the coordination number and λ is the electron mean free path.
[b]The R factor is the root-mean-square relative deviation, i.e., $R=[\sum_i(\chi_i-\chi_c)^2]^{1/2}/(\sum_i\chi_i^2)^{1/2}$.

plitudes), and that calculated from a 9-W-atom cluster with the WV_2O_6 structure.[49]

The cluster is assumed to be in the form of a plate with a diameter ($2R$) of 10 Å and a thickness of 1.5 Å, lying normal to the c axis of the rutile phase:

$$i(h)=[2/(hR)^2][1-J_1(2hR)/hR]\ . \qquad (11)$$

It is clear from this comparison that the SAXS data indicate that there are no W clusters; instead, the solute is distributed randomly. The curvature in the magnetic data at low fields must therefore arise because the material is a spin glass.

It is worth noting that a similar comparison with the

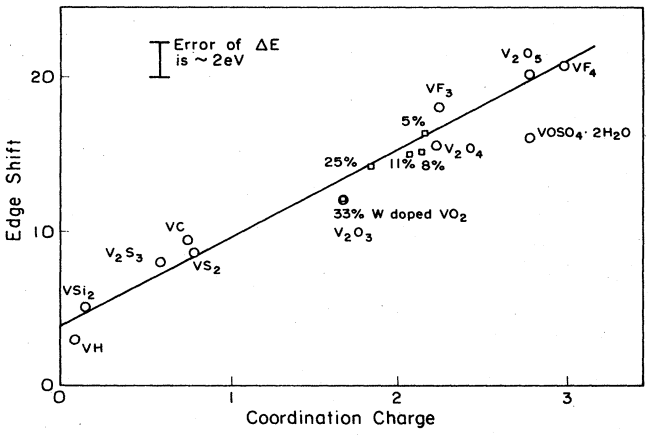

FIG. 11. Edge shift vs effective coordination charge. The effective coordination charge of $W_xV_{1-x}O_2$ (squares) is estimated as $\eta=(1-x)^{-1}[2x\eta(V^{3+})+(1-3x)\eta(V^{4+})]$.

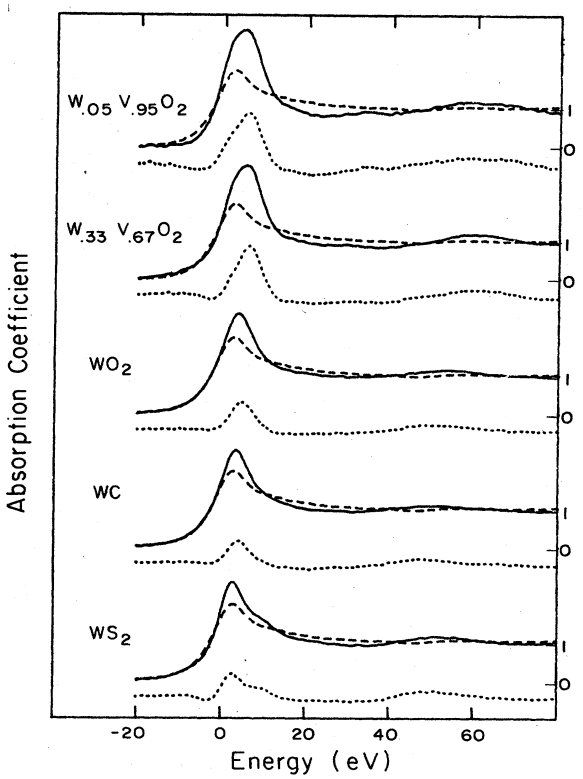

FIG. 12. Comparison of the L_{III}-edge resonances of W compounds (solid line) and W metal (dashed line). The difference spectrum (dotted line) of each compound is directly below. (Experiments were done on the in-lab EXAFS facility.)

TABLE VI. Ionicities, effective coordinate charges, and near-edge peak areas (W I_{III} edge), ΔA, for W compounds.

Compound	Ionicity	Effective coordination charge	ΔA (CHESS) (±0.5)	ΔA (in lab) (±0.5)
WO_2	0.29	1.16		4.3
WO_3	0.25	1.50	10.5	
WHO_4	0.25	1.50	10.3	
WC	0.21	0.084		3.2
WS_2	0.025	0.10		3.9
WV_2O_6	0.25	1.50	11.2	8.7
$W_{0.25}V_{0.75}O_2$	?		10.0	8.3
$W_{0.05}V_{0.95}O_2$	?		11.0	9.4

25% W-cation alloy revealed that the intensity was below that for a random solution. This implies that there is local order, in agreement with the magnetic data mentioned above, which suggested that at this composition there was local order similar to that in the antiferromagnetic phase, WV_2O_6.

Near-edge spectroscopy

The EXAFS spectra and RDF's taken (at CHESS) near the W L_{III} edge are shown in Fig. 9. The fitting parameters for the first two shells are given in Table V; the fit to the data is shown in Fig. 10. The Debye-Waller factor is much smaller for the 33% W-cation composition than for the more dilute alloys. In this case, the W ions are well ordered in the compound WV_2O_6, and static displacements are greatly reduced.

Included in Table V are the first-neighbor distances expected from the known lattice parameters. Based on these parameters, this distance is expected to increase with W content, but this does not actually occur. From published ionic radii,[50] a W-O distance of 2.02 Å would be expected for a W^{4+}-O^{2-} pair, and 1.94 Å would be expected for a W^{6+}-O^{2-} pair. This latter distance is close to the observed value in WV_2O_6, in which W is known to have a +6 valence, and close to the values in Table V. The second-neighbor distance (W-V pairs) is also close to the value expected for a W^{6+}-V^{3+} pair (2.98 Å). These data clearly support the interpretation of the magnetic data, namely that there is a valence change upon introducing W ions into VO_2.

The XANES spectra near the V K edge were examined (with the in-house facility). A series of V compounds, as well as the W alloys, were measured. The shifts in energy of the edge were analyzed in terms of the effective coordination charge η, following Lytle,[51]

$$\eta = mI \ , \tag{12}$$

where m is the valence of the absorber and I is the degree of ionicity defined by Pauling[52] as

$$I = 1 - \exp[-\tfrac{1}{4}(X_A - X_B)^2] \ . \tag{13}$$

Here, X_i is the electronegativity of species i. The shift in edge energy is plotted versus η in Fig. 11, where it can be seen that this shift decreases slightly with increasing W content. The direction of the shift suggests that at least some of the V ions have a charge of +3, but the evidence is not very conclusive. Accordingly, the pre-edge peak near the W L_{III} edge was investigated. The results are given in Table VI and Fig. 12, where some comparisons are given for data taken on the in-house facility as well as CHESS. It seems quite clear from these data that the valence of W is +6, since the area ΔA of the pre-edge peak for the alloys (above that for the metal) is twice that for WO_2, and close to that for WO_3.

CONCLUSIONS

We present the following conclusions:

(1) Upon doping VO_2 with W ions, the following reaction takes place:

$$2V^{4+} + W^{4+} \rightarrow 2V^{3+} + W^{6+} \ .$$

This is confirmed by magnetic measurements, EXAFS, and near-edge spectroscopy.

(2) As a result of this charge compensation, V^{3+}-V^{4+} and V^{3+}-W^{6+} pairs form. The former pair can denote one free electron, the other two being involved in a homopolar bond. The latter pair has two electrons to donate, so that the bonding between V and W ions is ionic for this pair.

(3) The loss of direct bonding between V ions lowers the temperature of the metal-insulator transition. A similar charge compensation occurs for Nb as a dopant.[16] Because each Nb^{+5} ion produces only one V^{3+}, the effect of doping on T_c should be half of that for a W^{+6} ion; this is the actual result.[7,17–24]

(4) The charge transfer also produces a spin glass because the W ions are randomly distributed in the structure.

ACKNOWLEDGMENTS

This research constitutes a portion of a thesis submitted (by C.T.) in partial fulfillment of the requirements for the Ph.D. degree at Northwestern University. Financial support was provided by the U.S. Army Research Office (ARO) under Contract No. DAAG-29-80-C-0035. The in-house x-ray studies were carried out in Northwestern University's x-ray facility, supported in part by the Northwestern University Materials Research Center under National Science Foundation (Materials Research Laboratories) Grant No. DMR-82-16972. We also thank Dr. D. Mills of CHESS for his advice and assistance.

[1]F. J. Morin, Phys. Rev. Lett. **3**, 34 (1959).
[2]C. H. Newman, A. W. Lawson, and R. F. Brown, J. Chem. Phys. **41**, 1591 (1964).
[3]K. Kosuge, J. Phys. Chem. Soc. Jpn. **22**, 551 (1967).
[4]G. Anderson, Acta Chem. Scand. **10**, 623 (1956).
[5]J. B. Goodenough, Bull. Soc. Chim. Fr. **4**, 1200 (1965).
[6]W. G. Rudorft, G. Walter, and J. Stodler, Z. Anorg. Allg. Chem. **297**, 1 (1958).
[7]T. Horlin, T. Niklewski, and M. Nygren, Mater. Res. Bull. **8**, 179 (1973).
[8]C. N. Berglund and H. J. Guggenheim, Phys. Rev. **185**, 1022 (1969).
[9]D. Adler and H. Brooks, Phys. Rev. **155**, 826 (1967).
[10]D. C. Mattis and N. Langer, Phys. Rev. Lett. **25**, 376 (1970).
[11]W. Paul, Mater. Res. Bull. **5**, 691 (1970).
[12]M. Gupta, A. J. Freeman, and D. E. Ellis, Phys. Rev. B **16**, 3338 (1977).
[13]J. B. Goodenough, Prog. Solid State Chem. **5**, 145 (1971).
[14]L. L. Vanzant, J. M. Honig, and J. B. Goodenough, J. Appl. Phys. **39**, 594 (1968).
[15]Z. Zinamon and N. F. Mott, Philos. Mag. **21**, 881 (1970).
[16]A. Zylbersztein and N. F. Mott, Phys. Rev. B **11**, 4383 (1975).
[17]J. B. MacChesney and J. B. Goodenough, J. Phys. Chem. Solids **30**, 225 (1969).
[18]T. Horlin, T. Niklewski, and M. Nygren, Mater. Res. Bull. **7**, 1515 (1972).
[19]O. Savborg and M. Nygren, Phys. Status Solidi A **43**, 645 (1977).
[20]J. P. Pouget, P. Lederer, D. S. Schreiber, H. Launois, D. Wohlleben, A. Casalot, and G. Villeneuve, J. Phys. Chem. Solids **33**, 1961 (1972).
[21]M. Nygren and M. Israelsson, Mater. Res. Bull. **4**, 881 (1969).
[22]P. Kleinschmidt, Phys. Lett. **47A**, 205 (1974).
[23]T. Horlin, T. Niklewski, and M. Nygren, Acta Chem. Scand. Ser. A **30**, 619 (1976).
[24]P. B. Febritchnyi, M. Bayard, M. Pouchard, and P. Hagenmuller, Solid State Commun. **14**, 603 (1974).
[25]T. Langill, Ph.D. thesis, Northwestern University, 1980.
[26]M. Israelsson and L. Kihlborg, Mater. Res. Bull. **5**, 19 (1970).
[27]H. Zijlstra, *Experimental Methods in Magnetism* (Elsevier, New York, 1967).
[28]V. Gerold and W. Schweizer, Z. Metallkd. **52**, 76 (1961).
[29]G. S. Knapp, H. Chen, and T. E. Klippert, Rev. Sci. Instrum. **49**, 1658 (1978).
[30]C. Tang, Ph.D. thesis, Northwestern University, 1983.
[31]P. Georgopoulos and C. Tang, Adv. X-ray Anal. **27**, 299 (1984).
[32]T. M. Hayes, P. N. Sen, and S. H. Hunter, J. Phys. C **9**, 4357 (1976).
[33]B. K. Teo and P. A. Lee, J. Am. Chem. Soc. **101**, 2815 (1979).
[34]G. Golub, Num. Math. **7**, 206 (1965).
[35]Y. Canchois and N. F. Mott, Philos. Mag. **40**, 1260 (1949).
[36]F. W. Lytle, P. S. P. Wei, R. B. Greegor, G. H. Via, and J. H. Sinfelt, J. Chem. Phys. **70**, 4849 (1979).
[37]J. C. Bernier, P. Poix, and M. G. Chaudron, C. R. Acad. Sci. Ser. C **265**, 1247 (1967).
[38]C. Kittel, *Introduction to Solid State Physics,* 4th ed. (Wiley, New York, 1972).
[39]I. S. Jacobs and C. P. Bean, *Magnetism III* (Academic, New York, 1963), p. 271.
[40]L. Néel, in *Low Temperature Physics Lectures delivered at University of Grenoble (Summer School of Theoretical Physics), 1961,* edited by C. DeWitt, B. Dreyfus, and P. G. de Gennes (Gordon and Breach, New York, 1962), p. 411.
[41]L. Néel, J. Phys. Soc. Jpn. Suppl. B1, **17**, 676 (1962).
[42]S. Mishra and P. A. Beck, Phys. Status Solidi A **19**, 267 (1973).
[43]P. A. Beck, Metall. Trans. **2**, 2015 (1971).
[44]J. J. Becker, Trans. Met. Soc. AIME **209**, 59 (1957).
[45]D. Sherrington and S. Kirkpatrick, Phys. Rev. Lett. **35**, 1792 (1975).
[46]P. Monod and H. Bouchait, J. Phys. (Paris) Lett. **43**, L45 (1982).
[47]G. E. Bacon, *Neutron Diffraction,* 3rd ed. (Oxford University Press, Oxford, 1975), p. 591.
[48]R. J. Weiss, Phys. Rev. **83**, 379 (1951).
[49]M. C. Montmory, E. F. Bertaut, and P. Mollard, Solid State Commun. **4**, 249 (1966).
[50]O. Kratky and G. Porod, J. Colloid. Sci. **4**, 35 (1949).
[51]F. W. Lytle (private communication).
[52]L. Pauling, *The Nature of the Chemical Bond,* 2nd ed. (Cornell University Press, Ithaca, New York, 1948).